OFFICE OF NAVAL RESEARCH

Grant # N00014-90-J-1167

R&T Code 4133019

Technical Report # 13

EQCM Studies of Film Growth, Redox Cycling, and Charge Trapping of n-Doped and p-Doped Poly(thiophene)

by

Ricardo Borjas and Daniel A. Buttry

Prepared for Publication in

Chemistry of Materials

Department of Chemistry
University of Wyoming
Laramie, WY 82071-3838

April 29, 1991

Unclassified

SECURITY CLASSIFICATION OF THIS PAGE

REPORT DOCUMENTATION PAGE

1a. REPORT SECURITY CLASSIFICATION Unclassified	1b. RESTRICTIVE MARKINGS
2a. SECURITY CLASSIFICATION AUTHORITY	3. DISTRIBUTION / AVAILABILITY OF REPORT Approved for public release and sale. Distribution unlimited.
2b. DECLASSIFICATION / DOWNGRADING SCHEDULE	
4. PERFORMING ORGANIZATION REPORT NUMBER(S) ONR Technical Report No. 13	5. MONITORING ORGANIZATION REPORT NUMBER(S)
6a. NAME OF PERFORMING ORGANIZATION University of Wyoming 6b. OFFICE SYMBOL (If applicable)	7a. NAME OF MONITORING ORGANIZATION Office of Naval Research Resident Representative
6c. ADDRESS (City, State, and ZIP Code) Department of Chemistry University of Wyoming Laramie, WY 82071-3838	7b. ADDRESS (City, State, and ZIP Code) University of New Mexico Bandelier Hall West Albuquerque, NM 87131
8a. NAME OF FUNDING / SPONSORING ORGANIZATION Office of Naval Research 8b. OFFICE SYMBOL (If applicable) ONR	9. PROCUREMENT INSTRUMENT IDENTIFICATION NUMBER N 00014-90-J-1167
8c. ADDRESS (City, State, and ZIP Code) 800 N. Quincy Street Arlington, VA 2217	10. SOURCE OF FUNDING NUMBERS PROGRAM ELEMENT NO. / PROJECT NO. / TASK NO. R+T 413301901 / WORK UNIT ACCESSION NO.

11. TITLE (Include Security Classification)

EQCM Studies of Film Growth, Redox Cycling, and Charge Trapping of n-Doped and p-Doped Poly(thiophene)

12. PERSONAL AUTHOR(S) R. Borjas and D.A. Buttry

13a. TYPE OF REPORT	13b. TIME COVERED	14. DATE OF REPORT (Year, Month, Day)	15. PAGE COUNT
Technical	FROM 9/90 TO 6/91	1991 April 29	30

16. SUPPLEMENTARY NOTATION

Submitted for publication in Chemistry of Materials

17 COSATI CODES			18. SUBJECT TERMS (Continue on reverse if necessary and identify by block number)
FIELD	GROUP	SUB-GROUP	electrochemistry, quartz crystal microbalance, conducting polymer

19. ABSTRACT (Continue on reverse if necessary and identify by block number)

Abstract - The electrochemical quartz crystal microbalance (EQCM) is used to monitor mass changes which accompany the growth, redox cycling, and charge trapping of thin films of poly(thiophene) (PT) at Au electrodes under potentiodynamic conditions. Mechanical conductance spectra of the EQCM/PT composite resonators reveal that the PT films behave as rigid layers, allowing use of the Sauerbrey equation for calculation of quantitative mass changes from the frequency changes recorded with the EQCM. Film growth by oxidation of 2,2'-bithiophene appears to proceed by production of soluble, short chain oligomers following oxidation, with precipitation a consequence of both reduction and increasing chain length.

(continued on back)

20. DISTRIBUTION / AVAILABILITY OF ABSTRACT ☒ UNCLASSIFIED/UNLIMITED ☐ SAME AS RPT ☐ DTIC USERS	21. ABSTRACT SECURITY CLASSIFICATION Unclassified
22a. NAME OF RESPONSIBLE INDIVIDUAL Daniel A. Buttry	22b. TELEPHONE (Include Area Code) (307) 766-6677 22c. OFFICE SYMBOL

DD FORM 1473, 84 MAR 83 APR edition may be used until exhausted. SECURITY CLASSIFICATION OF THIS PAGE

Evidence is presented for formation of isolated nuclei during the initial stages of film growth, followed by their coalescence after passage of approximately 0.5-1.5 mC cm-2 of oxidative charge during electropolymerization. Ellipsometry is used to verify film uniformity across the electrode surface for films with thicknesses between 300 and 1000 . Both the n-doping (reductive) and p-doping (oxidative) redox processes are studied in acetonitrile. Relatively stable n-doping is achieved by careful attention to solvent purity. Mass changes during redox cycling indicate that the predominant compositional changes which occur are anion insertion and expulsion during the p-doping process, and cation insertion and expulsion during the n-doping process although small amounts of solvent and/or supporting electrolyte are also transported in both processes. Charge trapping phenomena are observed for both then-doping and p-doping processes, with verification of simultaneous counterion trapping provided by the EQCM measurements.

EQCM Studies of Film Growth, Redox Cycling, and Charge Trapping of n-Doped and p-Doped Poly(thiophene)

Ricardo Borjas[a] and Daniel A. Buttry*

Department of Chemistry

University of Wyoming

Laramie, WY 82071-3838

Abstract - The electrochemical quartz crystal microbalance (EQCM) is used to monitor mass changes which accompany the growth, redox cycling, and charge trapping of thin films of poly(thiophene) (PT) at Au electrodes under potentiodynamic conditions. Mechanical conductance spectra of the EQCM/PT composite resonators reveal that the PT films behave as rigid layers, allowing use of the Sauerbrey equation for calculation of quantitative mass changes from the frequency changes recorded with the EQCM. Film growth by oxidation of 2,2'-bithiophene appears to proceed by production of soluble, short chain oligomers following oxidation, with precipitation as a consequence of both reduction and increasing chain length. Evidence is presented for formation of isolated nuclei during the initial stages of film growth, followed by their coalescence after passage of approximately 0.5-1.5 mC cm^{-2} of oxidative charge during electropolymerization. Ellipsometry is used to verify film uniformity across the electrode surface for films with thicknesses between 300 and 1000 Å. Both the n-doping (reductive) and p-doping (oxidative) redox processes are studied in acetonitrile. Relatively stable n-doping is achieved by careful attention to solvent purity. Mass changes during redox cycling indicate that the predominant compositional changes which occur are anion insertion and expulsion during the p-doping process, and cation insertion and expulsion during the n-doping process although small amounts of solvent and/or

supporting electrolyte are also transported in both processes. Charge trapping phenomena are observed for both the n-doping and p-doping processes, with verification of simultaneous counterion trapping provided by the EQCM measurements.

a) present address: Department of Chemistry, Memphis State University, Memphis, TN 38152.

* To whom correspondence should be addressed.

Introduction

Among the many possible applications of conducting polymers, they are especially attractive candidates for a variety of battery applications because of both the large amounts of charge which they can store and the sometimes high rates at which this charge can be extracted. In order to achieve high energy and power densities in these applications, the total mass of the cell must be carefully controlled without sacrifice in the rate of charge extraction. This requires a fairly detailed understanding of the transport processes which occur during redox cycling of conducting polymer films, coupled with practical strategies for their manipulation. We have previously described a poly(aniline)/Nafion composite film in which the charge compensating ionic transport during redox cycling was manipulated to achieve faster switching between the insulating and conducting states, a contribution demonstrative of such strategies (1). Monitoring of the ionic transport processes was accomplished with the electrochemical quartz crystal microbalance (EQCM), and their manipulation was achieved by fabrication of composite film structures.

The EQCM is an ideal tool for the study of compositional changes which occur during redox cycling in thin films of redox or conducting polymers. Several recent, detailed discussions of its use in such applications have appeared (2,3). It has been successfully applied to studies of the electropolymerization and redox cycling of several conducting polymers including poly(pyrrole) (4), poly(aniline) (5), poly(azulene) (6), poly(3-methylthiophene) (7), and poly(thiophene) (8). It has proven especially useful in the determination of the mechanism and efficiency of film growth for conducting polymers (4,5), redox polymer films (9), and other types of deposits (10), as well as in studies aimed at understanding transport of ions, solvent, and ion pairs or multiplets of supporting electrolyte species within such deposits (1,3,5,8,11-14). In the present contribution, the EQCM is used to study the growth of films of poly(thiophene) (PT) from bithiophene, the compositional changes which accompany the redox cycling of these films in both the n-doping and p-doping

cases, and charge trapping phenomena and consequent counterion trapping which result from a combination of n- and p-doping closely spaced in time.

Experimental

2,2'-bithiophene (BTH) was used for the electropolymerization of the films. Electropolymerization of thiophene was possible, but the EQCM results for this monomer suggested that dissolution of the underlying electrode material (both Au and Pt were investigated) was occurring at the very positive potentials required for oxidation of this monomer, which prompted the change to BTH. Acetonitrile (ACN) (Burdick and Jackson) was used as solvent. The solvent was kept as dry as possible by addition of activated alumina directly into the working electrode compartment of the cell. Tetrabutylammonium and tetramethylammonium hexafluorophosphates (TBAH and TMAH, respectively) were prepared and purified as previously reported (15), except that all were recrystallized either 4 or 5 times. $LiClO_4$ was carefully ground to a fine powder, spread evenly over a watchglass, and dried at 100 °C under vacuum for 72 hours, then cooled under vacuum and transferred directly to the electrochemical cell. The cell was of conventional design (H-cell), except that a glass #9 vacuum o-ring joint was blown onto its side to allow for the EQCM crystal to be sandwiched between two o-rings in such a way that only one side was exposed to the solution. Also, the cell contained a Luggin capillary to reduce the uncompensated resistance between the working and reference electrodes. The reference electrode was a Ag wire immersed in a solution of the supporting electrolyte containing 0.04 M $AgClO_4$, separated from the working compartment by a porous glass plug. Ferrocene appears at $+0.08 \pm 0.01$ V versus this reference. All potentials are reported versus this Ag/Ag^+ reference. Supporting electrolyte was 0.1 M unless otherwise stated, and monomer solutions were 0.05 M.

Films were prepared under potentiodynamic (i.e. cyclic voltammetric) conditions, with potential limits of 0.0 and 0.8 V. The solution was typically agitated between scans by

action of the purging gas (Ar). Film thickness and uniformity were determined by ellipsometry (Rudolf Research, Auto El). In the dry state, film thicknesses were typically between 300 and 1000 Å, with the uniformity always better than ±15 Å and ±50 Å, respectively. Good uniformity is important in EQCM studies because the mass sensitivity across the face of the EQCM crystal electrode has a rather strong dependence on the radial distance from the center of the EQCM electrode (2).

The EQCM apparatus has been described (2). It allows measurement of mass changes at the electrode surface by virtue of linearly proportional changes in the resonant frequency of the composite resonator comprised of the EQCM crystal and the polymer film deposited onto it. The sensitivity is more than adequate for monitoring compositional changes in the multilayer films investigated here. For this measurement, frequency decreases correspond to mass gain, and vice versa, with the proportionality constant, C_f, for our instrument being 56.6 Hz cm^2 μg^{-1}. The instrumentation for the mechanical impedance measurements has also been previously described (2,13). Briefly, the impedance measurement consists of the application of an alternating voltage of precisely defined frequency, and measurement of the phase and amplitude of the alternating current which flows through the crystal as a consequence of the applied voltage. The resolution for these measurements was typically 20 Hz. These measurements are used to compute various quantities of interest, including the conductance, G (in Ω^{-1} cm^{-1}) and the frequency of maximum conductance, f_{max} (in Hz), which provides a measure of the total mass deposited during electropolymerization of a given film (2). In order to apply the Sauerbrey equation to these films for quantitative calculation of mass changes from frequency changes, it must first be demonstrated that the film behaves rigidly. This is best done by demonstrating that the width of the peak in the conductance spectrum does not change when the film is deposited (2,13). Below are reported Δf_{fwhh} (i.e. full width at half height of the the conductance peak in Hz) values which verify that PT behaves rigidly under the experimental conditions used here.

Results and Discussion

Film Growth and Rigidity

Table 1 shows how the values of Δf_{fwhh} and f_{max} vary with the number of scans into the potential region in which electropolymerization occurs for a PT film which was electropolymerized in 0.1 M TBAH in ACN with 0.05 M BTH at a scan rate of 50 mV s^{-1}. These values were measured at an applied potential of 0.0 V, where the film is in its insulating, undoped state. The constancy of Δf_{fwhh} with increased film thickness (i.e. the more scans, the thicker the film) shows that the film behaves rigidly under these conditions. Thus, the decrease in f_{max} (for a total frequency decrease of 230 Hz) measures the total accumulation of mass at the surface caused by electropolymerization, which was 4.1 x 10^{-6} g cm^{-2}. Note that this mass change was measured after poising the electrode potential back to a value at which the polymer was undoped (i.e. neutral) so it represents only the mass of deposited PT plus any supporting electrolyte which might be incorporated into the neutral form of the film.

Table 2 shows similar data for another film. In this case, the Δf_{fwhh} values were also determined under potential control at +0.85 V (i.e. in the conducting, oxidized or p-doped state) and at -2.33 V (i.e. in the conducting, reduced or n-doped state). The data reveal that the film is also rigid in its p-doped state, but not in its n-doped state, although the deviation of the Δf_{fwhh} value from that for the rigid state is much less than has been observed for other types of films (13,16). In such a case, quantitative calculations of mass changes from frequency data must be interpreted with some caution. The precise origin of these slight deviations from rigid film behavior in the n-doped state is unclear at this time. However, it may be related to the relative chemical instability of the film in its n-doped state (e.g. a significant degree of chain cleavage might be expected to induce non-rigid behavior) and the considerable length of time required for obtaining the conductance spectrum (ca. 5 minutes).

Figure 1 shows an EQCM scan into the potential region in which electropolymerization occurs for a virgin Au electrode. The CV (curve A) shows classic nucleation loop behavior, as expected based on previous studies of PT electropolymerization which indicated nucleation to be a prominent effect in the growth of these films (17-19). The EQCM frequency response (curve B) shows that a small mass gain occurs following scan reversal, but that the majority of the mass gain from this first electropolymerization scan occurs at potentials near those at which the p-doped material is reduced back to the neutral, insulating state. The magnitude of the frequency decrease during the first scan will be discussed below.

Figure 2 shows the tenth scan during the electropolymerization of this film. The redox process for the film which was formed during the previous nine scans is observed, as is the mass gain (loss) due predominantly to anion insertion (expulsion) during oxidation (reduction). In addition to the features from the previously formed film, the net frequency decrease during the scan reveals that additional film has been deposited. Very similar data have previously been reported for a study of the electropolymerization of poly(aniline) (5).

These observations suggest that the process of PT film growth requires that oligomers of sufficient size must be formed prior to the initiation of deposition, and that the solubility of the oligomers is much lower in the neutral than in the p-doped state. These notions are in accord with previous studies of PT electropolymerization (17-19) which indicated that film formation occurs by formation of oligomers which deposit when they reach a critical value (3-4 units), and that further growth probably occurs from these nuclei. Christensen et al. (20) used FTIR to study PT deposition and redox cycling, and found that the thiophene monomer does not adsorb appreciably at Au, again, in support of the need for deposition of oligomers (via insolubility) to form nucleation points for further growth.

Another indication of the formation of nuclei in the early stages of film deposition is given by the data in Table 3. These data show the variation of the effective mass of the

leposit as a function of the number of scans into the region of electropolymerization. The key quantities to compare are the experimentally measured charge consumed in a given scan, Q_{ex}, and the net frequency decrease for a given scan, Δf_{ex}. These values are used to calculate two effective masses, m_1 and m_2, respectively, in the following way:

$$m_1 = Q_{ex}\, MW_{BT} / n\, F \qquad (1)$$

$$m_2 = \Delta f_{ex} / C_f \qquad (2)$$

where MW_{BT} is the molar mass of bithiophene, n is the number of electrons required to deposit a BT unit into the polymer, and F is the Faraday constant. The value of n contains implicitly both the electropolymerization charge efficiency and the electron stoichiometry for film deposition. A value of 2.0 was assumed for these calculations.

The data in Table 3 are best represented as the ratio of m_2/m_1. This ratio provides a measure of the degree to which the deposition process makes efficient use of the electrochemical charge consumed in the oxidation of the BT monomer. Inefficient use of the charge would lead to values of m_2/m_1 less than 1.0. This ratio also provides information about the morphology of the deposit. It has been previously shown that, for cases in which the deposit morphology is rough enough to cause trapping of supporting electrolyte within pores or between nuclei of the deposit, the mass changes which are calculated from the observed frequency changes can be much larger than expected (2,10). In the present case, these phenomena would be manifested by a value for m_2/m_1 which is larger than 1.0. It can be seen that for the first few scans, m_2/m_1 is much larger than 1.0, consistent with the production of isolated nuclei which trap considerable amounts of supporting electrolyte between them. However, as the number of scans increases, this ratio approaches 1.0, indicating that a) the current efficiency for the electropolymerization process is near to 1.0, and b) the morphology of the deposit is such that there is not significant trapping of supporting electrolyte within the film. This variation of the ratio m_2/m_1 with number of scans is exactly what would be expected for the production of isolated nuclei which merge

after further growth, and is consistent with the observations reported above and by previous investigators (17-20).

Redox Cycling

Figures 3 and 4 show EQCM scans into the regions for p-doping (oxidation) and n-doping (reduction), respectively, in a solution containing only supporting electrolyte. The observation of stable n-doping has only been reported a few times (22-24), and requires careful attention to solvent and supporting electrolyte purity, especially with regard to water content. Also, we note is passing that the presence of even traces of alkali metal cations in the supporting electrolyte (either intentionally added material or adventitious impurities) causes relatively rapid destruction of the n-doped state. The frequency changes observed during the scans reveal that both doping processes are accompanied by pronounced mass increases, and both undoping processes by mass loss. The hysteresis in the voltammetry is mimicked in the mass changes. Feldberg and coworkers have recently proposed a model for such unusual quasi-reversible (UQR), hysteretic behavior based on phase transformations which accompany the redox process (21). It seems likely that the insertion of anions during the p-doping and cations during the n-doping processes may be responsible for the phase transformations responsible for this UQR behavior, as pointed out by Feldberg.

Direct comparison of the CV data with the mass data is facilitated by the representation of the mass data in a derivative format (2,8,10). This method of visualizing the data relies on the direct connection of the removal (insertion) of electrons during the doping process(es) with the insertion of anions (cations), and vice versa during the undoping processes. In this way, subtle differences between the electron and ion transport processes are more easily seen. Figures 5 and 6 show such plots for the p-doping and n-doping of PT, respectively. The salient feature of the plots is that the mass transported during the redox process is significantly larger than that predicted for simple, unidirectional transport of charge-compensating ions. Hillman et al. have analyzed such behavior in depth for PT films

prepared in a slightly different way (8). In the present case, it suffices to say that this "extra" mass is undoubtedly due to incorporation of small amounts of salt and/or solvent during the doping processes and their expulsion during undoping back to the insulating state.

The mass changes and the charges for cycling several films through their p-doping and n-doping transitions were measured as functions of scan rate. These data are reported in Table 4. From 25 to 100 mV s^{-1}, the mass changes and charges were constant for p-doping. On the other hand, both quantities decreased with increasing scan rate for the n-doping process, as shown in the table. The difference in redox cycling transport behavior between the n-doped and p-doped states has been attributed to differences in counterion diffusion rates for the two processes in PT (22). However, both TBAH and TMAH gave identical results in the present case, indicating that the identity of the cation does not play a major role in determining the transport rates. Rather, we attribute the difference to the much lower conductivity of the n-doped state compared to the p-doped state (22,24), and the consequent decrease in charge propagation rate via electron hopping.

Charge Trapping Behavior

Murray and coworkers (25) have studied the charge trapping effect for bilayers of several different types of polymer systems. The effect is essentially a type of rectification caused by mismatch between the redox potentials of the inner and outer films. In most cases, one of the key criteria for observation of such effects is a redox polymer for the inner film with more than one stable redox couple, so that charging and discharging can occur at separate redox potentials. In cases of this type the phenomenon is conceptually straightforward, and it has been used in a variety of elegant experiments to measure various parameters of interest regarding redox polymer films (25). However, the phenomenon has also been observed in films which are thought of as uniformly homogeneous, such as poly(3-methylthiophene) (22). We have also observed this phenomenon for PT films, and discuss the behavior below.

Figure 7 shows a CV of PT in which the negative scan was initiated at 0.0 V, but after first having been scanned into the potential region for p-doping (this initial part of the scan is not shown for clarity). The peak marked A on the CV appears as a prewave on the peak for the n-doping process and corresponds to the release of p-doped charge which had been trapped in the film while in its neutral state. Similarly, the peak marked B appears as a prewave on the peak for the p-doping process. It corresponds to the release of n-doped charge which had been trapped in the film while in its neutral state. These prewaves are not observed unless the film had recently been scanned to the opposite potential extreme of the scan. The magnitude of the peaks decreases considerably with time, so that they are only observed when the scan to the opposite potential extreme has been fairly recent (e.g. within several minutes).

Figure 8 shows a plot of charge versus potential for the CV in Figure 7. The releases of the trapped charge are marked as A and B, to correspond with the markings in Figure 7. Note that after the second charge trapping peak (curve B, Figure 7) has been traversed, the charge returns to its original value. This demonstrates that charge is completely conserved during the cathodic process (i.e. all of the trapped charge is recovered, and there is no significant amount of electrolysis of residual impurities). Symmetric results are observed for the case of an initially positive scan direction. The difference between the initial and final charges in Figure 8 is a measure of the amount of charge trapped in the positive scan. It is numerically quite similar to the amount trapped during the negative scan. Also, the amount of trapped charge in both the negative and positive scans is quite large, equalling about 30% of the total charge for the anodic process and 25% of the total charge for the cathodic process.

Figure 9 shows the mass changes which are observed during these charge trapping events. In the negative scan, there is a slow, but significant increase of frequency prior to the prewave. We believe this is caused by the slow release of some of the trapped p-doped charge, and a consequent loss of anions. Close inspection of Figure 8 reveals a corresponding

slow increase in charge in the same potential region, consistent with this interpretation. An intriguing result is that the frequency change marked A (i.e. from prewave A in Figure 7) corresponds to a mass gain rather than a mass loss. This must indicate that the predominant process here is cation insertion as opposed to anion expulsion. The detrapping event marked B appears to correspond to a simple release of cations. The frequency attains its original value, indicating that the mass changes which occur during these charge trapping and detrapping events are chemically reversible.

An interesting question to address about these data relates to the cause of the cation insertion during the cathodic detrapping event (prewave A). Anion expulsion would seem to be the more preferred process, both because of free volume considerations and because, for the most part, charge compensation in conducting polymers seems to occur by more or less unidirectional transport processes which nearly obey Donnan exclusion. In other words, p-doping processes are predominantly accompanied by anion transport and n-doping processes are predominantly accompanied by cation transport. However, there is precedent for effects such as the one observed here (23,26). For example, in the first EQCM study of a conducting polymer, Kaufman and coworkers (26) observed a similar effect during the undoping of poly(pyrrole) in 0.1 M $LiClO_4$ in tetrahydrfuran solvent. In their case, p-doping was accompanied by ClO_4^- insertion, but undoping was accompanied by Li^+ insertion rather than ClO_4^- expulsion. This was attributed to strong ion pairing between the cationic sites on the p-doped poly(pyrrole) chains and the ClO_4^- anions, induced by the very low dielectric constant within the film interior. The solvent was implicated in the behavior, because no such effect was observed when ACN was used as solvent. We suspect a similar origin for the effects we have observed for PT films. Thus, strong ion pairing between cationic, p-doped sites on the PT chains and their PF_6^- counterions may cause cation insertion rather than anion expulsion during the detrapping event marked A. However, we have no information regarding whether this event is a kinetic or thermodynamic consequence of such ionic

interactions. Scan rate studies would seem to be a relatively simple way to determine this, but the instability of the charge trapped state of PT precludes such experiments at scan rates low enough to perhaps observe deviations from the behavior observed so far. However, we speculate that the effect is predominantly kinetic, both because of free volume arguments (i.e. cation insertion requires swelling of the film) and because studies by us and others indicate that, at equilibrium, neutral PT films do not contain much solvent or supporting electrolyte (8,18-20). Also, whatever the origin of these effects, they must be sensitive to the chemical nature of the anion and cation, because the mass transport processes which occur during detrapping are not symmetric for the n- and p-doped states.

Conclusions

These EQCM studies of film growth, redox cycling, and charge trapping in PT have demonstrated that 1) film growth occurs by nucleation and eventual coalescence of the initially formed nuclei, a process which is easily observed with the EQCM (2,10), 2) the mass transport processes which occur during redox cycling are predominantly, but certainly not exclusively (8), accompanied by permselective, unidirectional ion transport to achieve charge compensation, and 3) that charge trapping/detrapping events occur for PT films, and that the EQCM method provides a rather unique tool with which to study these processes.

The observation of ion transport in unexpected directions during detrapping of p-doped charge leads one to conclude that strong ionic interactions prevail inside these low dielectric constant media, and that these interactions can influence the charge compensation processes which occur for films of conducting polymers and other materials which require ionic charge compensation. Understanding and manipulating these ionic interactions will be important in many applications of these materials because of the known dependence of conductivity on ion pairing (the so-called "charge-pinning" effect) (27).

Another interesting aspect of these data is that the charge trapped during n- and

p-doping is very similar and fairly large with respect to the total doping charge. This large degree of charge trapping may have important practical implications for applications requiring rapid charge/discharge cycles, but it may also reveal something about the relative homogeneity of these films. For example, the fact that the charge trapped during n- and p-doping is very similar in magnitude may suggest that this charge is trapped in the same region(s) of the film, suggesting the possibility of considerable heterogeniety within the film. Trapping via a homogeneous mechanism (e.g. trapping by isolation from the underlying electrode by the intervening polymer layer which becomes insulating first during the undoping process(22)) seems unlikely in this case, because it should depend on the film conductivities, which are known to be at least two orders of magnitude different for the n- and p-doped cases (22,24). Also, careful ellipsometric studies of the mode of doping for poly(aniline), another (albeit, different) conducting polymer system, indicate uniform doping and undoping (28). Another factor which argues against trapping via a homogeneous mechanism involving the presence of an insulating layer near the electrode is that large electric fields would be generated across this layer, which would act to accelerate the motion of electrons or holes across it in a direction which would defeat the charge trapping process. Thus, in the present case, trapping via a mechanism involving film heterogeniety seems more likely. We suggest that there are regions of these films which are in relatively poor physical contact with the bulk of the film, and that the deswelling (caused by ion expulsion) which occurs during the undoping process causes the bulk of the film to draw away from these regions, thus degrading the quality of the electronic contact between them. On doping at the opposite potential extreme, reswelling (due to ionic insertion) occurs, re-establishing the electronic contact needed for efficient release of the trapped charge.

While this suggestion that charge trapping in such materials is caused by film heterogeniety is clearly of a speculative nature, it does suggest that microscopic investigations of such films are in order. Such studies are facilitated by the ability to make

various types of spectroscopic measurements with relatively high spatial resolution, such as FTIR, Raman, fluorescence, etc. We hope that this report will prompt such investigations.

Acknowledgements

We are grateful to the Office of Naval Research for the full support of this work.

References

1. Orata, D.; Buttry, D.A. J. Electroanal. Chem., 1988, 257, 71-82.
2. Buttry, D.A. In Electroanalytical Chemistry. A Series of Advances., Bard, A.J., Ed.; Marcel Dekker: New York, 1991; Vol. 17, pp. 1-85.
3. Buttry, D.A. In In-Situ Studies of Electrochemical Interfaces, Abruna, H., Ed.; VCH: New York, 1991; in press.
4. Baker, C.K.; Reynolds, J.R. J. Electroanal. Chem., 1988, 251, 307-22.
5. Orata, D.; Buttry, D.A. J. Am. Chem. Soc., 1987, 109, 3574-81.
6. Borjas, R.; Buttry, D.A., manuscript in preparation.
7. Servagent, S.; Vieil, E. J. Eletroanal. Chem., 1990, 280, 227-32.
8. Hillman, A.R.; Swann, M.J.; Bruckenstein, S. J. Electroanal. Chem., 1990, 291, 147-62.
9. Hillman, A.R.; Loveday, D.C.; Bruckenstein, S. Langmuir, 1991, 7, 191-94.
10. Ostrom, G.S.; Buttry, D.A. J. Electroanal. Chem., 1988, 256, 411-31.
11. Hillman, A.R.; Loveday, D.C.; Bruckenstein, S. J. Electroanal. Chem., 1989, 274, 157-65.
12. Varineau, P.T.; Buttry, D.A. J. Phys. Chem., 1987, 91, 1292-95.
13. Borjas, R.; Buttry, D.A. J. Electroanal. Chem., 1990, 280, 73-90.
14. Lasky, S.J.; Buttry, D.A. J. Am. Chem. Soc., 1988, 110, 6258-60.
15. Fry, A.J.; Britton, W.E. In Laboratory Techniques in Electroanalytical Chemistry, Kissinger, P.T.; Heineman, W.R., Eds.; Marcel Dekker: New York, 1984, Chapter 13.

16. Varineau, P.T.; Buttry, D.A., unpublished data.

17. Hillman, A.R.; Mallen, E.F. J. Electroanal. Chem., 1987, 220, 351-67.

18. Hamnett, A.; Hillman, A.R. Ber. Bunsenges. Phys. Chem,, 1987, 91, 329-36.

19. Lang, P.; Chao, F.; Costa, M.; Lheritier, E.; Garnier, F. Ber. Bunsenges. Phys. Chem., 1988, 92, 1528-36.

20. Christensen, P.A., Hamnet, A.; Hillman, A.R. J. Electroanal. Chem., 1988, 242, 47-62.

21. Feldberg, S.W.; Rubinstein, I. J. Electroanal. Chem., 1988, 240, 1-15.

22. Crooks, R.M.; Chyan, O.M.R.; Wrighton, M.S. Chem. Mater., 1989, 1, 2-4.

23. Mastragostino, M.; Soddu, L. Electrochim. Acta, 1990, 35, 463-66.

24. Kaneto, K.; Ura, S.; Yoshino, K.; Inuishi, Y. Jpn. J. Appl. Phys., Part 2, 1984, 23, 189-91.

25. see, for example, Murray, R.W. In Electroanalytical Chemistry. A Series of Advances., Bard, A.J., Ed.; Marcel Dekker: New York, 1984; Vol. 13, pp. 191-368.

26. Kaufman, J.N.; Kanazawa, K.K.; Street, G.B. Phys. Rev. Lett., 1984, 53, 2461-64.

27. Frommer, J.E. J. Macromol. Sci. Chem., 1987, A24, 449-454.

28. Gottesfeld, S.; Redondo, A.; Feldberg, S. J. Electrochem. Soc., 1987, 134, 271-72.

Table 1

Conductance Data for PT Film During Film Growth[a]

Scan Number	Δf_{fwhh}(Hz)	f_{max}(MHz)
0	1180	4.950609
4	1180	4.950579
43	1180	4.950379

a) 0.1 M TBAH + 50 mM BTH in ACN. Scan number 0 corresponds to a conductance spectrum taken prior to film growth. The working electrode was at an applied potential of 0.0 V for these measurements.

Table 2

Potential Dependent Conductance Data for PT Film During Growth[a]

Scan Number	Δf_{fwhh}(Hz)
0	1080
1	1080
3	1080
10	1080
10A	1080
10B	1220

a) 0.1 M TBAH + 50 mM BTH in ACN. Scan number 0 corresponds to a conductance spectrum taken prior to film growth. All conductance spectra were taken under potential control at 0.0 V, expect 10A and 10B which were taken at +0.85 V and -2.33 V, respectively.

Table 3

Relation of Charge and Frequency Change for Individual Scans During Electropolymerization[a]

υ(mV/s)	Scan Number	Q_{ex}(mC/cm^2)	Δf_{ex}(Hz)	m_2/m_1
50	1	0.16	210	26
50	5	0.31	51	3.0
50	10	0.70	40	1.2
25	1	0.60	448	15
25	3	0.80	168	4.3
25	6	2.4	121	1.0

a) 0.1 M TBAH + 50 mM BTH in ACN. υ is scan rate. Data are for two different films prepared at two different scan rates.

Table 4

Charges and Frequency Changes During Redox Cycling for N- and P-Doping

υ(mV/s)	Δf_n(Hz)	Q_n(mC/cm^2)	Δf_p(Hz)	Q_p(mC/cm^2)
25	280	1.95	180	1.44
50	210	1.50	190	1.40
100	175	1.35	180	1.40

Figure Captions

1. EQCM data for first scan of electropolymerization of BTH. 0.1 M TBAH + 50 mM BTH in ACN; scan rate = 50 mV/s. CV - curve A. QCM - curve B.
2. EQCM data for tenth scan of electropolymerization of BTH. 0.1 M TBAH + 50 mM BTH in ACN; scan rate = 50 mV/s. CV - curve A. QCM - curve B.
3. EQCM data for thin film of PT in pure 0.1 M TBAH in ACN; scan rate = 50 mV/s; p-doping process. CV - curve A. QCM - curve B.
4. EQCM data for thin film of PT in pure 0.1 M TBAH in ACN; scan rate = 50 mV/s; n-doping process. CV - curve A. QCM - curve B.
5. EQCM data for thin film of PT in pure 0.1 M TBAH in ACN; scan rate = 50 mV/s; p-doping process. Dashed curve is CV; solid curve is the derivative of the frequency with potential. See text for details.
6. EQCM data for thin film of PT in pure 0.1 M TBAH in ACN; scan rate = 50 mV/s; n-doping process. Dashed curve is CV; solid curve is the derivative of the frequency with potential. See text for details.
7. CV data showing charge trapping phenomena for PT in pure 0.1 M TMAH in ACN; scan rate = 50 mV/s. Initial potential = 0.0 V; initial scan direction is negative. A scan over the p-doping wave (i.e. up to +0.8 V and back to 0.0 V) occurred just prior to this scan. See text for explanations of peaks A and B.
8. Charge versus potential for the scan shown in Figure 7.
9. Frequency versus potential for the scan shown in Figure 7.

Fig 2

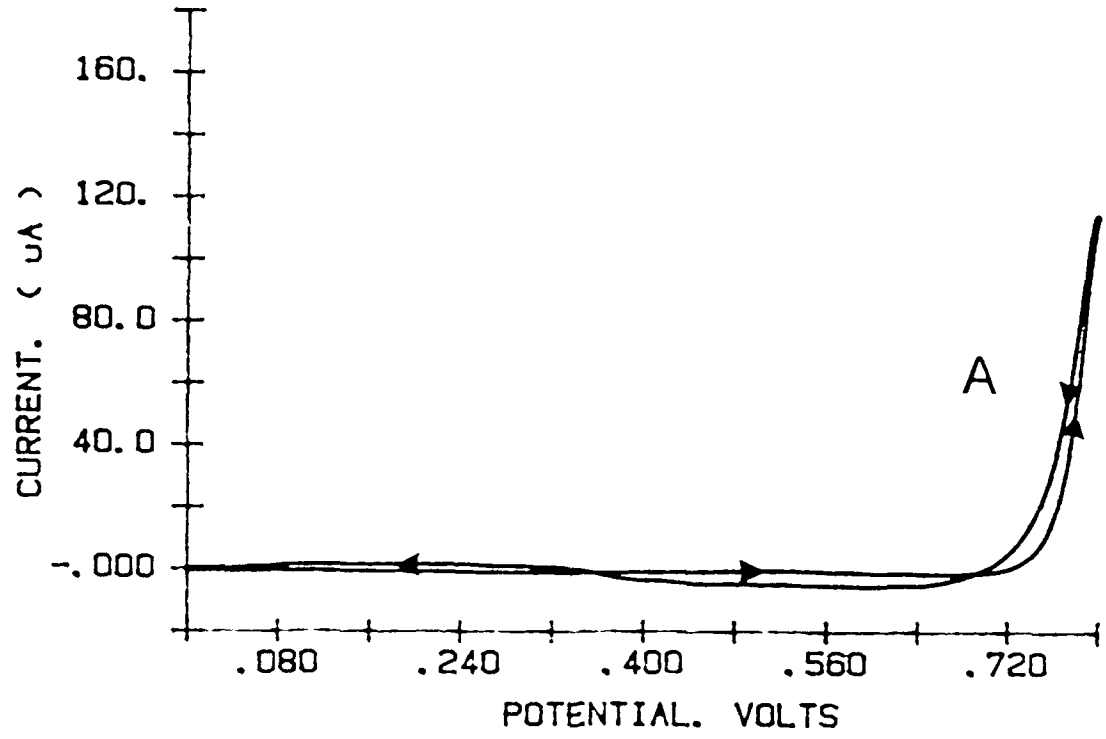
160.
120.
80.0
40.0
-.000
CURRENT. (uA)
A
.080
.240
.400
.560
.720
POTENTIAL. VOLTS

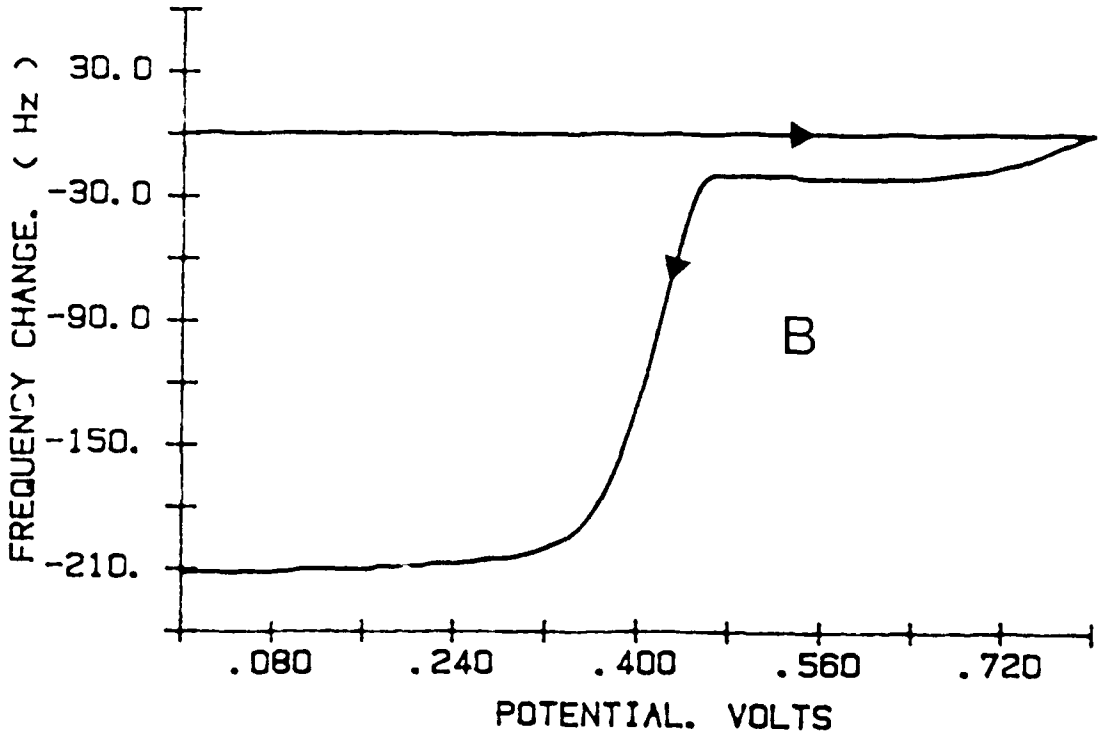
30.0
-30.0
-90.0
-150.
-210.
FREQUENCY CHANGE. (Hz)
B
.080
.240
.400
.560
.720
POTENTIAL. VOLTS

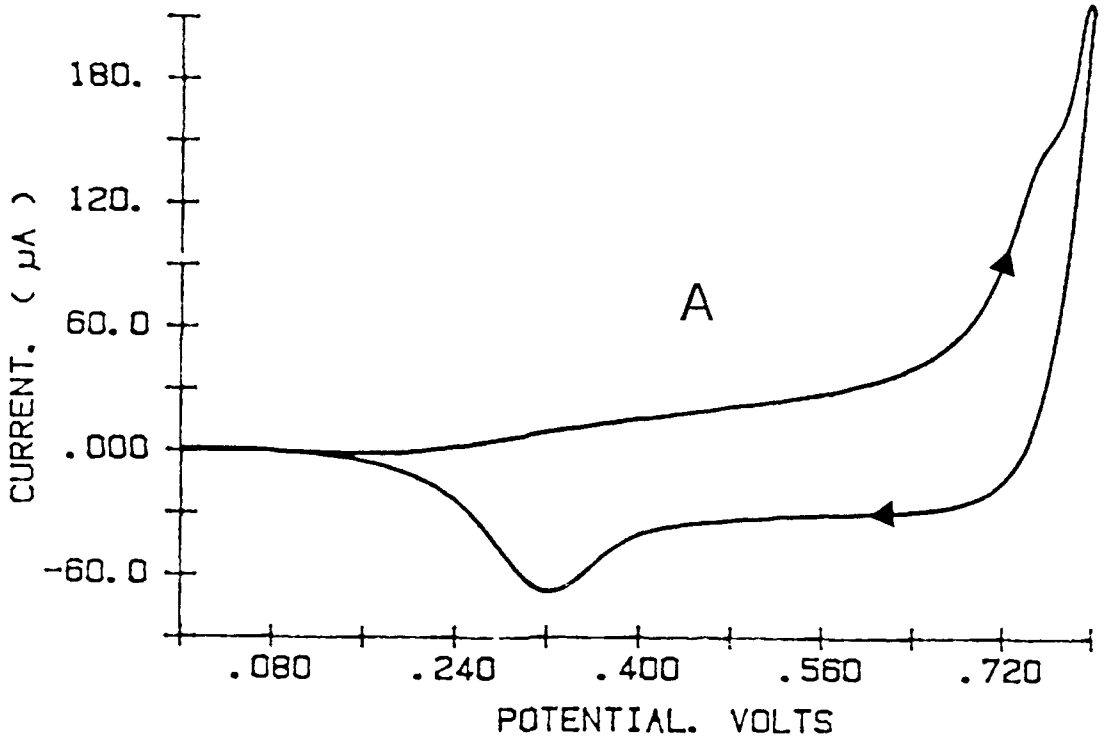
180.
120.
60.0
.000
-60.0
CURRENT. (μA)
A
.080
.240
.400
.560
.720
POTENTIAL. VOLTS

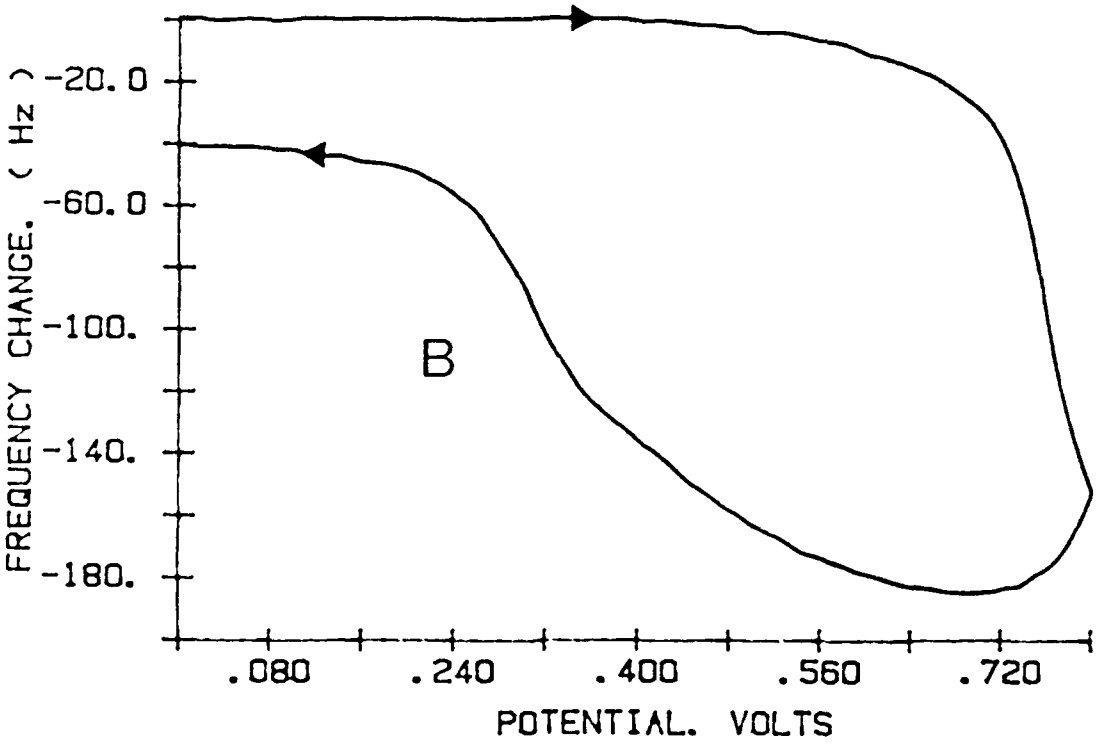
-20.0
-60.0
-100.
-140.
-180.
FREQUENCY CHANGE. (Hz)
B
.080
.240
.400
.560
.720
POTENTIAL. VOLTS

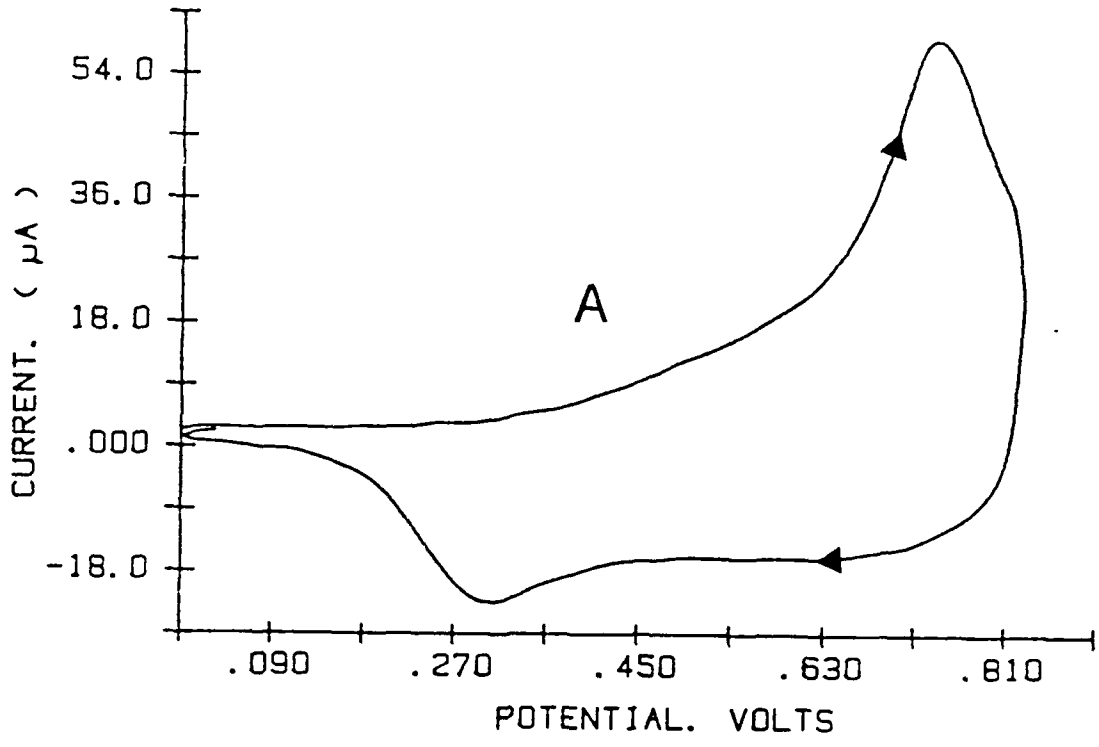
54.0
36.0
18.0
.000
-18.0
CURRENT. (μA)
A
.090
.270
.450
.630
.810
POTENTIAL. VOLTS

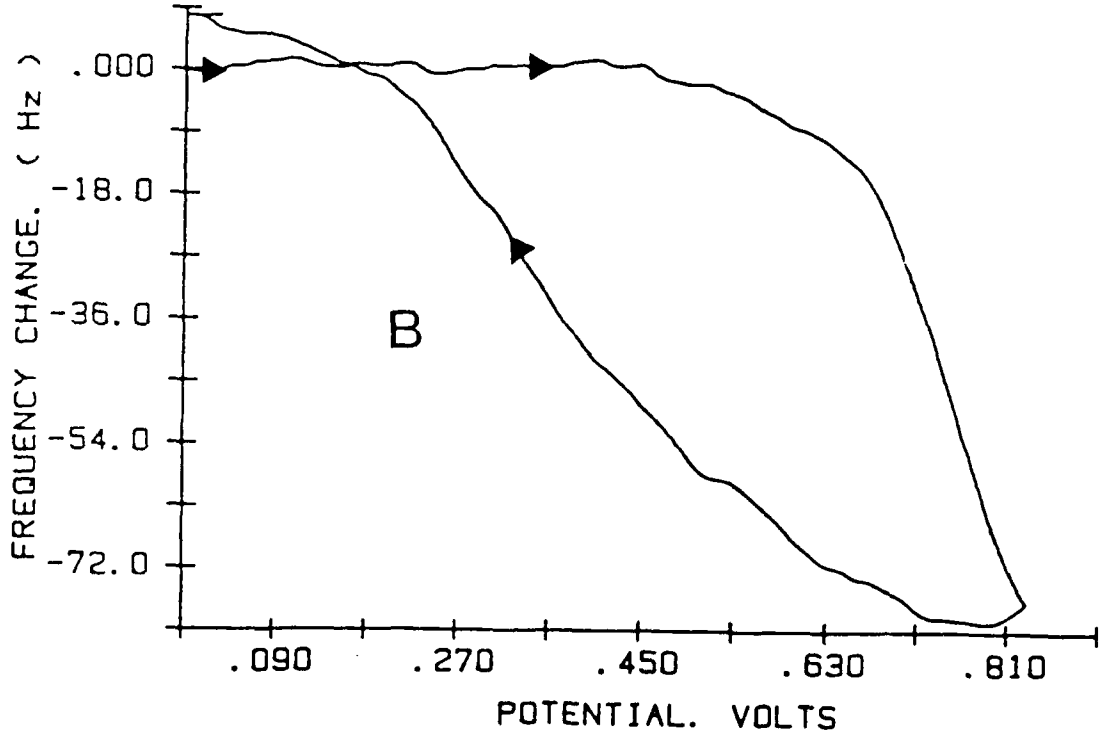
.000
-18.0
-36.0
-54.0
-72.0
FREQUENCY CHANGE. (Hz)
B
.090
.270
.450
.630
.810
POTENTIAL. VOLTS

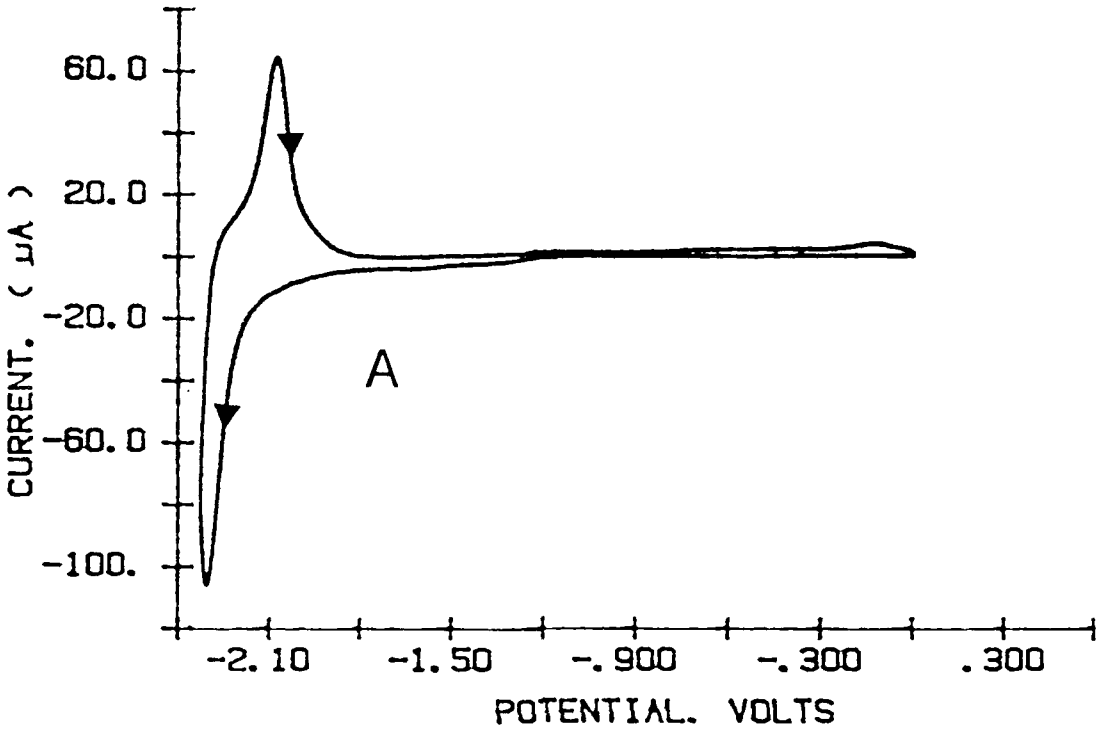
60.0
20.0
-20.0
-60.0
-100.
CURRENT. (μA)
A
-2.10
-1.50
-.900
-.300
.300
POTENTIAL. VOLTS

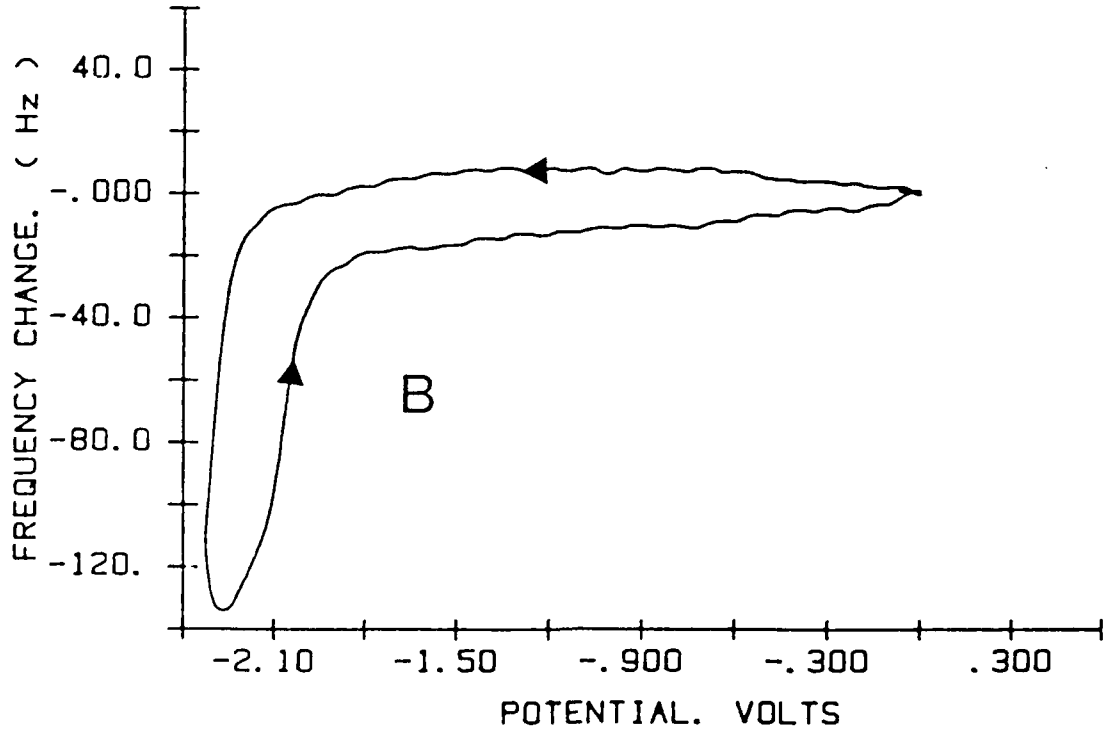
40.0
-.000
-40.0
-80.0
-120.
FREQUENCY CHANGE. (Hz)
B
-2.10
-1.50
-.900
-.300
.300
POTENTIAL. VOLTS

Fig 5

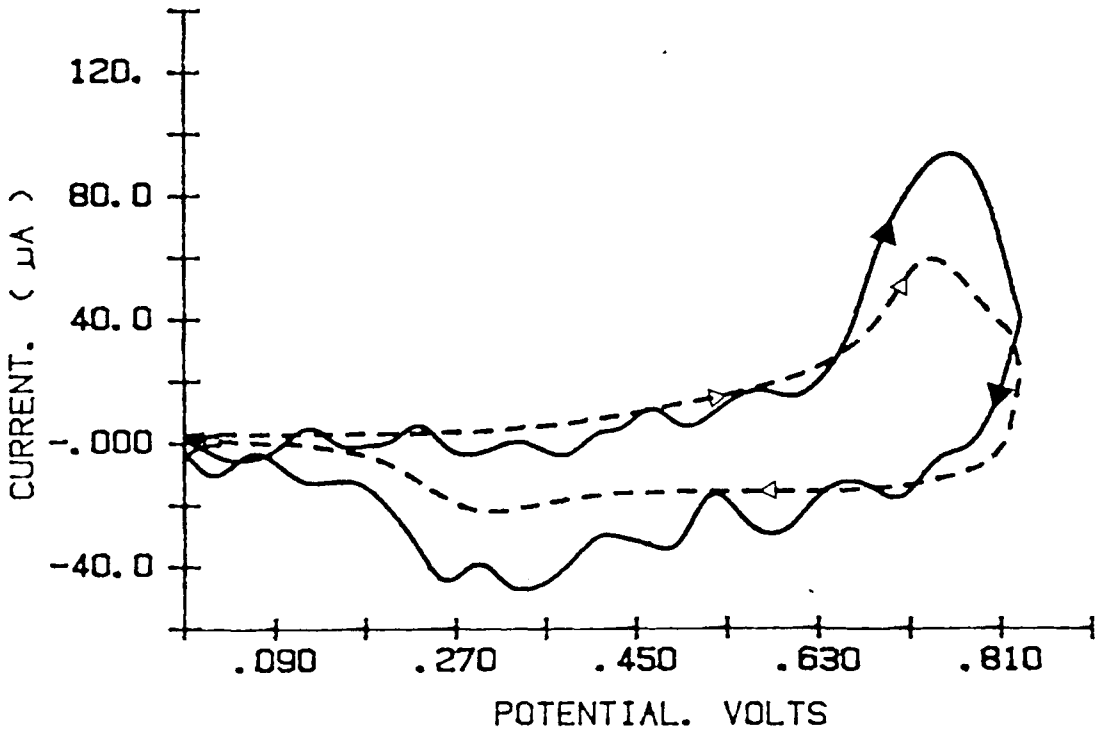
120.
80.0
40.0
-.000
-40.0
CURRENT. (μA)
.090
.270
.450
.630
.810
POTENTIAL. VOLTS

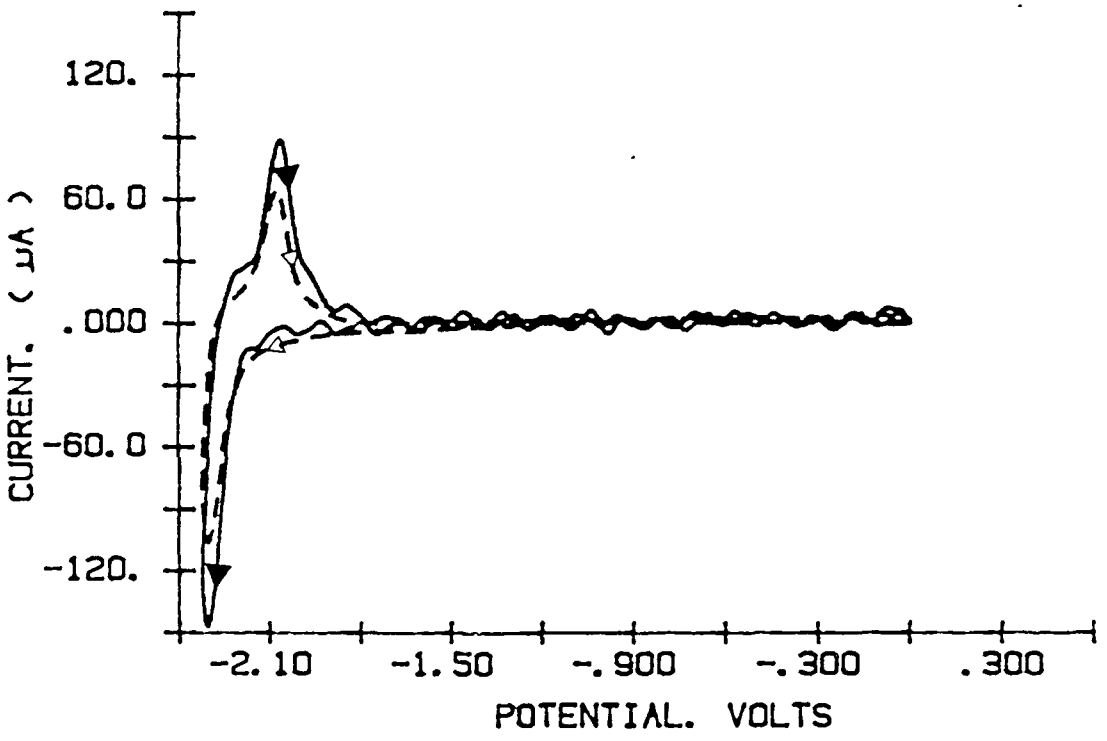
120.
60.0
.000
-60.0
-120.
CURRENT. (μA)
-2.10
-1.50
-.900
-.300
.300
POTENTIAL. VOLTS

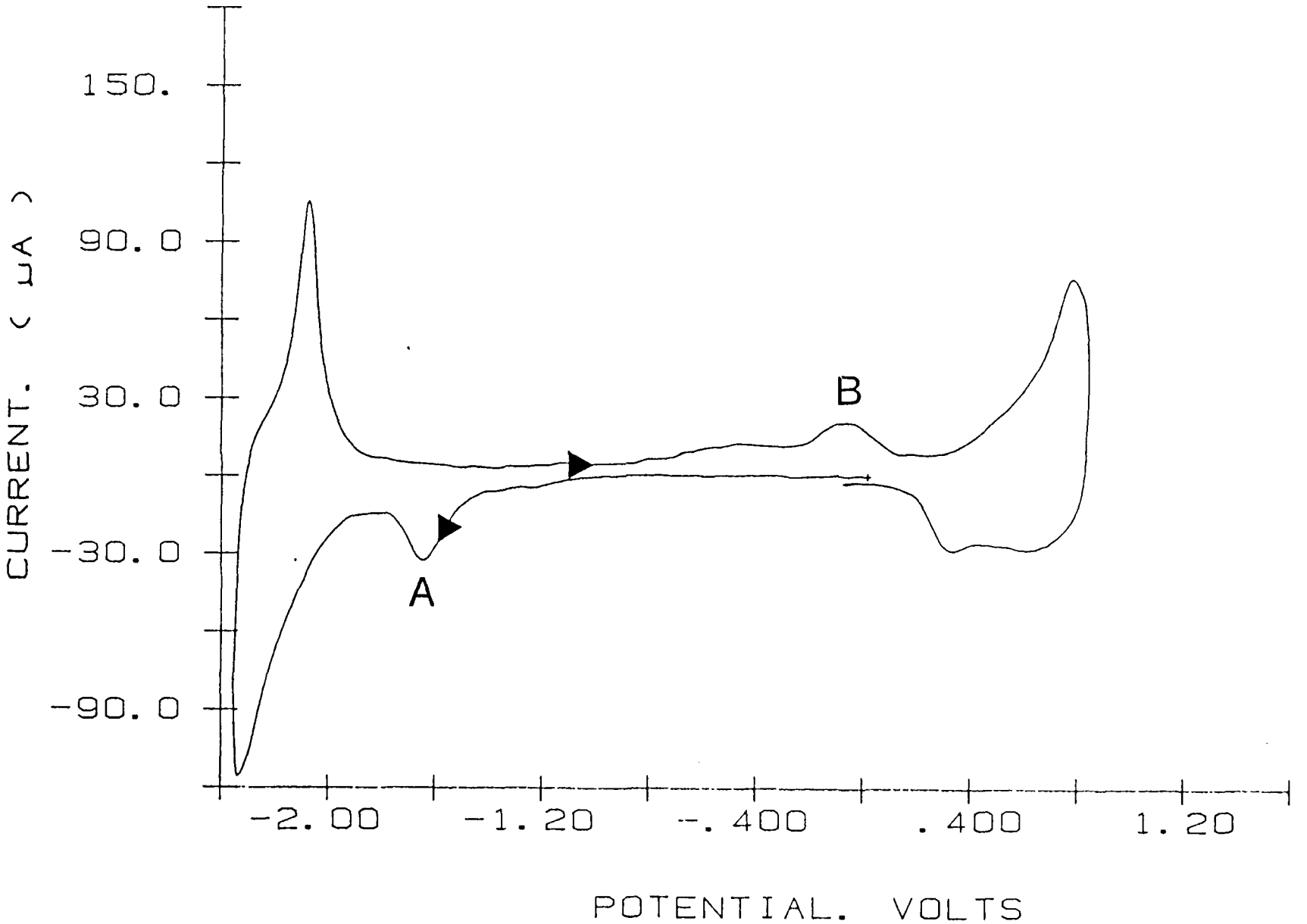
150.
90.0
30.0
-30.0
-90.0
CURRENT. (μA)
A
B
-2.00
-1.20
-.400
.400
1.20
POTENTIAL. VOLTS

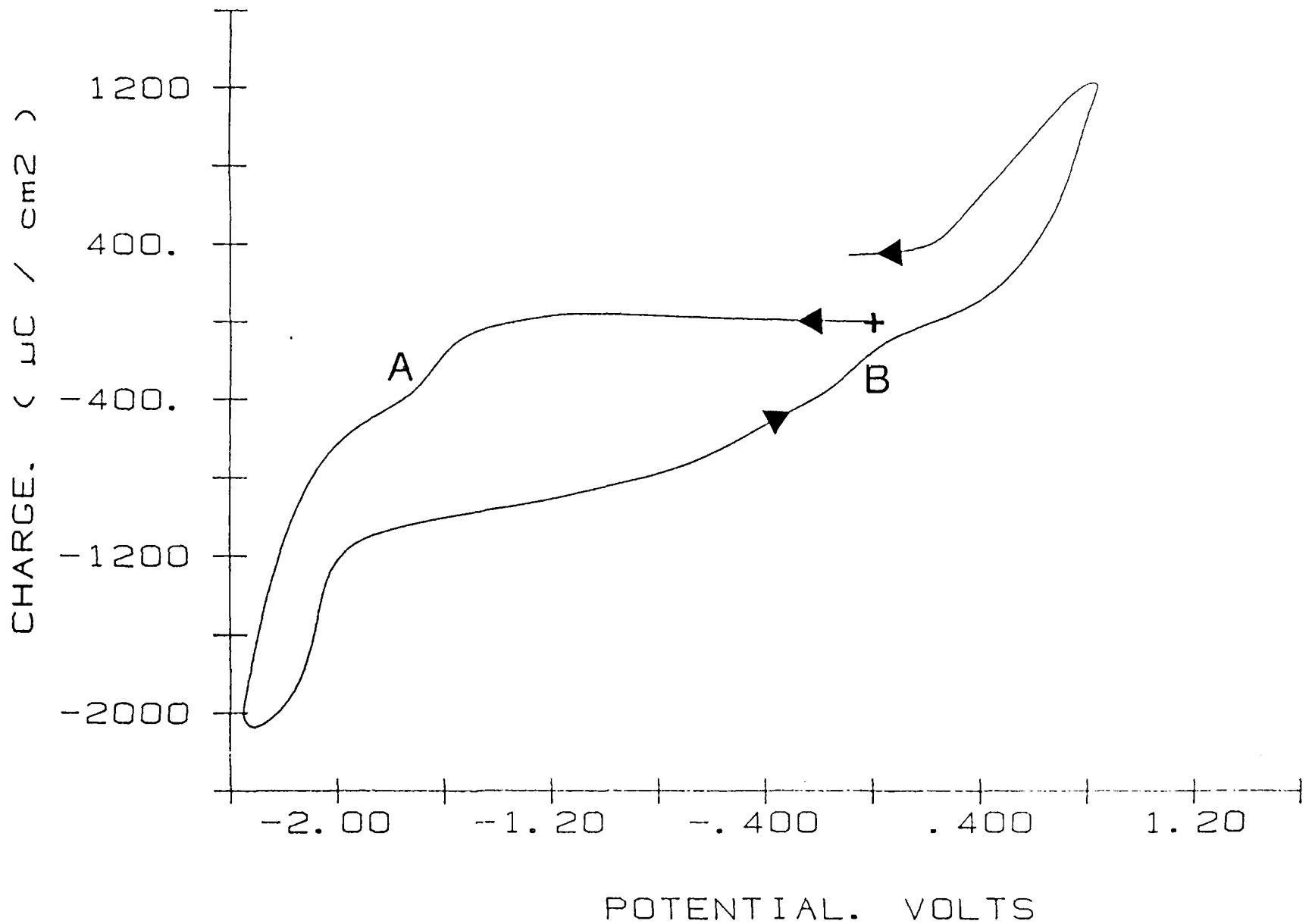
1200
400.
-400.
-1200
-2000
CHARGE. (µC / cm2)
A
B
-2.00
-1.20
-.400
.400
1.20
POTENTIAL. VOLTS

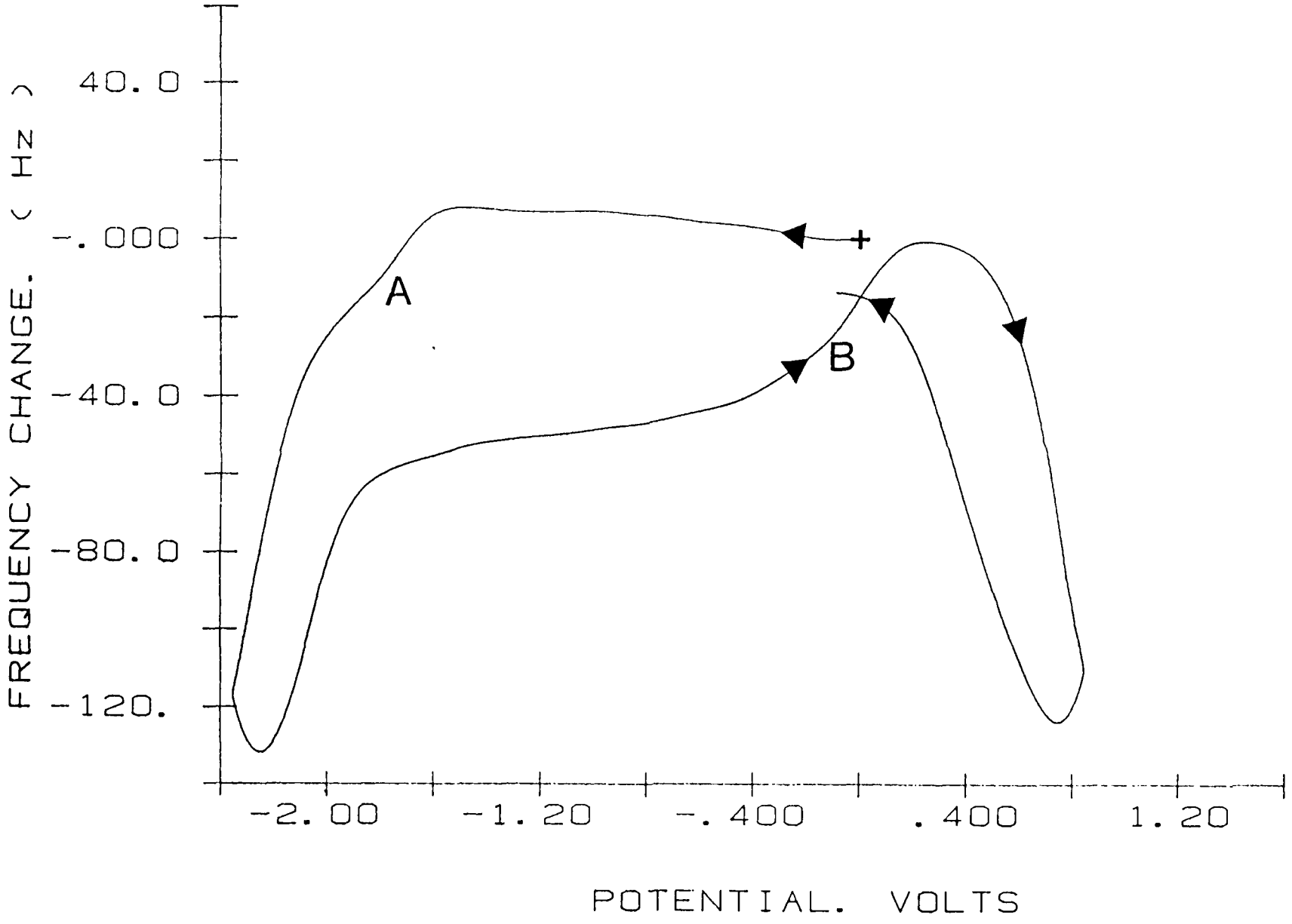
40. 0
-. 000
-40. 0
-80. 0
-120.
FREQUENCY CHANGE. (Hz)
A
B
-2. 00
-1. 20
-. 400
. 400
1. 20
POTENTIAL. VOLTS